CATO project: WP 5, activity 3, no. 11 and 12 (5.3.11/12)

Method development and method description using Durham ultrasonic data (Imaging method validation by means of numerical simulations and ultrasonic lab measurements)

*D.D. Šijačić *, J. Spetzler, K.H.A.A. Wolf*
TU-DELFT

ABSTRACT

This report describes development of time-lapse monitoring method and its validation. Our aim is to newly developed 4D crosswell tomography validate not only on synthetic but also on ultrasonic data. To obtain needed crosswell data two types of modelling experiments are considered: *i)* 2D finite-difference (FD) modelling and *ii)* 3D ultrasonic modelling of a time-lapse system.

Time-lapse tomographic method is first validated using synthetic data obtained by 2D FD modeling. Numerical modeling simulates ultrasonic experiment where ultrasonic broadband waveform data were recorded in a crosswell setting at the laboratory of University of Durham. Two data sets have been obtained from two almost identical physical models simulating pre-flood and post-flood stages during an enhanced oil recovery. We have applied a time-lapse method based on ray theory and wave scattering theory to estimate velocity differences thereby induced.

The variations of the time-lapse tomographic method, i.e., how the observed traveltimes shifts are estimated and which type of inversion (ray of wave theory based) is used, result with several different time-lapse velocity tomograms. What is new is that we work with time-lapse tomography using time delays directly, instead of separately performing inversions of the first and second survey estimating velocity structure and then differencing those tomograms in order to obtain the 4D velocity model. We compare here results of this standard time-lapse monitoring approach and of our new way to directly estimate 4D velocity structure.

At the end, applications of our 4D method on real field data sets, and on a new ultrasonic experiment simulating CO_2 injection in the subsurface, are discussed.

INTRODUCTION

We investigate time-lapse (also known as 4D) tomography which is a seismic monitoring technique, using synthetic and ultrasonic crosswell data. Synthetic data are obtained from 2D numerical simulations of the ultrasonic wave experiment, using finite-difference method.

*Delft University of Technology, Department of Geotechnology, email: D.Sijacic@tudelft.nl

Next, instead of setting a real field crosswell configuration and obtaining seismic data, we work with ultrasonic data obtained from the scaled physical model. Physical modeling is considered to be an attractive way of obtaining realistic 3D and 4D seismic data, though numerical modeling is still the most popular. The advantage of the physical modeling is that it is not based on algorithms but on the laws of physics. Hence, the wave propagation is real. Like in numerical modeling, the subsurface is completely known but one does not have to deal with the realms of approximations within wave equation itself (high-frequency approximation, acoustic rather than full elastic, 2D instead of 3D etc.) or boundary conditions or algorithm limitations (discretizing continuous reality) or limitations in the computer power and memory.

In physical modeling the seismic measurements are simulated on a laboratory scale. A scale model of the subsurface can be made from materials like rubbers, epoxies, plastics, metals, ceramics, etc. The seismic measurements are carried out with small sources and detectors, made from piezo-electric materials, using ultrasonic frequencies. The scaling factor is in the order of thousands (or tens of thousands). Physically modelled data can be recorded in real acquisition geometry as well as in a time-lapse mode. The source and detector motion is in 3D so that crosswell or any other acquisition geometry can be simulated.

Seismic data recorded in seismic experiments contain mostly low-frequency components because the Earth acts as a low-pass filter. High-resolution velocity models estimated in inversions based on ray theory may be considerably biased because ray theory is a high-frequency approximation of the wave theory. To obtain correct high-resolution images, it is instead better to apply tomographic inversion methods based on wave theory, because the finite-frequency effect of waves is taken into account.

The structure of this report is as follows: First, a method for 4D monitoring by crosswell tomographic wavefield inversion is presented. Thereafter, an ultrasonic experiment from the University of Durham is described. The model from Durham experiment is also used for our numerical modeling. To obtain synthetic data which are used for the validation of our 4D tomographic method, we preform 2D FD modeling. Then, we present results of 2D and 3D modeling. Images with the estimated time-lapse velocity are result of traveltime shift inversion using both standard ray theory and finite-frequency wave theory. Furthermore several variations of our 4D monitoring approach are discussed. Finally, we draw conclusions and discuss possible seismic applications of this method.

METHODOLOGY FOR 4D MONITORING

In this section, we present a time delay tomographic method used in a time-lapse mode in order to monitor 4D changes. Also, here we outline a linear finite-frequency wave theory (as well known as scattering theory) for the traveltime variation of propagating wavefields in complex media wherein single scattering of waves is included because it is used in the tomographic wavefield inversion process.

For the certain source-receiver distance ($\mathbf{r}_s$ is the source position and $\mathbf{r}_r$ is the receiver position), to the first order of the approximation travel time of the first arrivals can be represented as (Snieder and Sambridge (1992)):

$$t_1(\mathbf{r}_r, \mathbf{r}_s) = t_{ref}(\mathbf{r}_r, \mathbf{r}_s) + \Delta t_1(\mathbf{r}_r, \mathbf{r}_s) \tag{1}$$

where $t_{ref}(\mathbf{r}_r, \mathbf{r}_s)$ is the reference travel time of first arriving P-waves through an arbitrary reference velocity model. $\Delta t_1(\mathbf{r}_r, \mathbf{r}_s)$ is the travel time perturbation inherent to the velocity perturbation $\Delta v_1(\mathbf{r})$ of the reference velocity field $v_{ref}(\mathbf{r})$ at coordinate position $\mathbf{r}$. Namely, any velocity field can be represented as a sum of a reference field and some small perturbation on top of it. Therefore, the baseline velocity field $v_{base}(\mathbf{r})$ to the first order of the approximation is written as

$$v_{base}(\mathbf{r}) = v_{ref}(\mathbf{r}) + \Delta v_1(\mathbf{r}) \tag{2}$$

Following the same logic, for the second, monitoring survey, the travel time of the first arrivals can be written as

$$t_2(\mathbf{r}_r, \mathbf{r}_s) = t_{ref}(\mathbf{r}_r, \mathbf{r}_s) + \Delta t_2(\mathbf{r}_r, \mathbf{r}_s) \ , \tag{3}$$

while the monitoring velocity field can be represented using the same reference velocity field as in the first survey as

$$v_{mon}(\mathbf{r}) = v_{ref}(\mathbf{r}) + \Delta v_2(\mathbf{r}). \tag{4}$$

The monitor time delay Δt_2 is the time shift from the velocity perturbations with respect to the reference velocity field. That velocity perturbation may be represented as:

$$\Delta v_2(\mathbf{r}) = \Delta v_1(\mathbf{r}) + \Delta v_{4D}(\mathbf{r}) \tag{5}$$

Therefore, the monitoring time delay consists of the baseline time delay Δt_1 and the 4D time delay Δt_{4D} inferred from the changes in the target velocity field $\Delta v_{4D}(\mathbf{r})$ between the baseline and monitoring survey

$$\Delta t_2(\mathbf{r}_r, \mathbf{r}_s) = \Delta t_1(\mathbf{r}_r, \mathbf{r}_s) + \Delta t_{4D}(\mathbf{r}_r, \mathbf{r}_s) \tag{6}$$

Furthermore, since we use the identical reference model in both surveys, we can simply subtract Eq. (1) from Eq. (3) to obtain time difference between first arrivals in monitor and baseline wavefields, i.e., to obtain the velocity differences between the two models,

$$\Delta t_{4D}(\mathbf{r}_r, \mathbf{r}_s) \equiv \Delta t(\mathbf{r}_r, \mathbf{r}_s) = \Delta t_2(\mathbf{r}_r, \mathbf{r}_s) - \Delta t_1(\mathbf{r}_r, \mathbf{r}_s) \ . \tag{7}$$

The traveltime shift $\Delta t(\mathbf{r}_r, \mathbf{r}_s)$ and amplitude variation $\Delta A/A_0(\mathbf{r}_r, \mathbf{r}_s)$ of the scattered field with respect to the reference field are derived from the imaginary and real part, respectively, of the exponential function in the following equation for the Rytov wavefield $P_R(\mathbf{r}_r, \mathbf{r}_s, \omega)$ at the angular frequency $\omega = 2\pi\nu$

$$P_R(\mathbf{r}_r, \mathbf{r}_s, \omega) = P_0(\mathbf{r}_r, \mathbf{r}_s, \omega) \exp\Big(\frac{P_B}{P_0}(\mathbf{r}_r, \mathbf{r}_s, \omega)\Big), \tag{8}$$

where $P_0(\mathbf{r}_r, \mathbf{r}_s, \omega)$ is the reference wavefield inherent to the reference velocity model $v_0(\mathbf{r})$ and $P_B(\mathbf{r}_r, \mathbf{r}_s, \omega)$ is the first order Born wavefield. To model wavefields we use Rytov approximation which accounts for the single-scattering process of a propagating wavefield in heterogeneous media, for more details in derivation, see Aki and Richards (1980); Woodward (1992); Snieder and Lomax (1996); Spetzler and Snieder (2001).

To the first order of the approximation (i.e., a single-scattering approach), the traveltime delay can be expressed as a volume integration over the target image area V of the sensitivity function $K_{\Delta t}(\mathbf{r})$ times the velocity perturbation field $\Delta v(\mathbf{r})$

$$\Delta t(\mathbf{r}_r, \mathbf{r}_s) = \int_V \Delta v(\mathbf{r}) K_{\Delta t}(\mathbf{r}) dV, \tag{9}$$

while the relative amplitude variation is

$$\frac{\Delta A}{A_0}(\mathbf{r}_r, \mathbf{r}_s) = \int_V \Delta v(\mathbf{r}) K_{\Delta A}(\mathbf{r}) dV. \tag{10}$$

The sensitivity functions $K_{\Delta t}(\mathbf{r})$ and $K_{\Delta A}(\mathbf{r})$ are known as Fréchet kernels for the traveltime shift and amplitude variation. The Fréchet kernel depends on the source-receiver geometry, the reference model, and includes the broadband frequency characteristics of the recorded wavefield. The integration is carried out over the volume V between the source and receiver. A detailed derivation of Eq. (9) and (10) is given by Aki and Richards (1980), Snieder and Lomax (1996) and Spetzler and Snieder (2001).

For wave propagation in 2D, the Fréchet kernel for traveltime shift is described by

$$\begin{aligned} K^{2D}_{\Delta t}(x,z) &= -\sqrt{\frac{L}{v_0^5 x(L-x)}} \int_{\nu_0-\Delta\nu}^{\nu_0+\Delta\nu} A(\nu) \\ &\quad \times \sqrt{\nu} \sin\left(\frac{\nu\pi L z^2}{v_0 x(L-x)} + \frac{\pi}{4}\right) d\nu, \end{aligned} \tag{11}$$

in a homogeneous reference medium of the constant velocity v_0 and with the 2D coordinate $\mathbf{r} = (x, y)$. The source-receiver distance $L = |\mathbf{r}_r - \mathbf{r}_s|$, and the frequency is denoted by ν. The sensitivity kernel is integrated over the frequency band $[\nu_0 - \Delta\nu; \nu_0 + \Delta\nu]$ and the normalised amplitude spectrum $A(\nu)$ satisfies $\int_{\nu_0-\Delta\nu}^{\nu_0+\Delta\nu} A(\nu)\, d\nu = 1$. Further on in this paper, we discuss only traveltime components, though in a similar way, amplitude components can be easily derived too (plots of sensitivity kernels for amplitude perturbations can be found in Aki and Richards (1980); Snieder and Lomax (1996)). Here, we constrain our validation study only to traveltime tomography because the travel time attribute is more reliable than the amplitude attribute (i.e., possible unknown parameters are the source-receiver coupling, attenuation and the geometrical spreading factor).

For 3D wave propagation in a homogeneous reference model, the Fréchet kernel for traveltime residuals is equal to

$$\begin{aligned} K^{3D}_{\Delta t}(x,y,z) &= -\frac{L}{v_0^3 x(L-x)} \int_{\nu_0-\Delta\nu}^{\nu_0+\Delta\nu} A(\nu) \\ &\quad \times \nu \sin\left(\nu\pi L \frac{(y^2+z^2)}{v_0 x(L-x)}\right) d\nu, \end{aligned} \tag{12}$$

where the 3D coordinate $\mathbf{r} = (x, y, z)$. This equation can also be found in Hung *et al.* (2001) and Spetzler *et al.* (2002).

An example of sensitivity kernels for transmitted waves in a crosswell configuration is illustrated in Fig.1. These Fréchet kernels are calculated using the physical parameters in the Durham laboratory experiment which will be described in more detail in the next section. The offset between the vertical array of sources and receivers is 46.5 m, the frequency range of the transmitted waves goes from 200 Hz to 500 Hz and the reference velocity model is indicated in the Fig.2. The sensitivity kernels (shades of blue, white and red) are smooth functions since the finite-frequency effect of waves is taken into account. The Fresnel zones (edge of the white and blue colour) for the finite-frequency waves and the ray paths (solid yellow line) are also visible in the figure. The Fresnel zones correspond well to the central

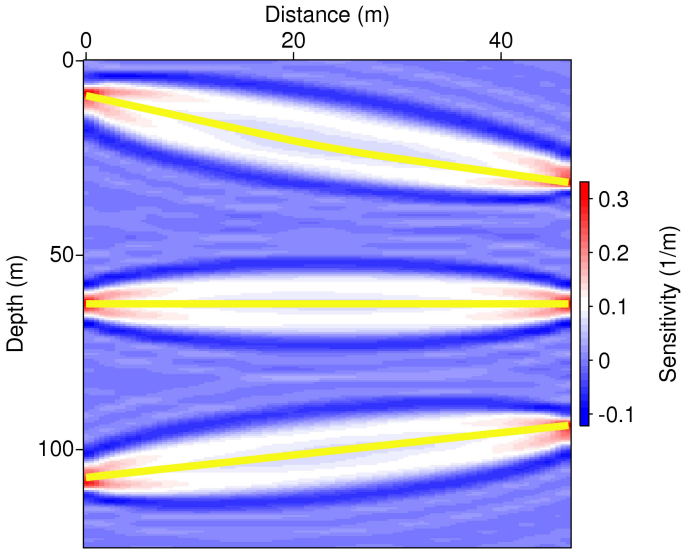

Figure 1: An example of Fréchet kernels calculated within finite-frequency wave theory and of ray paths in a crosswell setting for the case of the Durham ultrasonic experiment.

width of the sensitivity kernels. Because of the high-frequency approximation applied in ray theory, the sensitivity to slowness perturbations vanishes at positions off the ray path.

In a similar vein to Eq. (9), the traveltime shift derived from ray theory is a line integration of the slowness perturbation field along the ray path from the source to the receiver point. One can derive the ray theoretical result for traveltime shifts from Eq. (9) because the Fréchet kernel $K(\mathbf{r})$ converges to a delta function in the high-frequency limit. Thereby, the volume integration is reduced to a line integration. Thus,

$$\lim_{f\to\infty} \Delta t(\mathbf{r}_r, \mathbf{r}_s) = -\int_{ray} \frac{\Delta v}{V_{ref}^2}(\mathbf{r})\, d\mathbf{r}\ . \tag{13}$$

Scattering theory for traveltimes of waves is important in media where the Fresnel zone $L_F = \sqrt{\lambda L}$ is larger than the length-scale a of heterogeneities, in the contrast to ray theory which is valid only for media where $\lambda/a < 1$ and $L_F/a < 1$ (λ is the dominant wavelength and L denotes the length of the ray path). Hence, scattering theory is natural extension of ray theory and it is valid for

$$\frac{L_F}{a} > 1. \tag{14}$$

An illustration of the validity of expression (14) can be found in Fig. 4 and 5 of Spetzler and Snieder (2001).

To summarise, this section outlines the methodology for 4D tomography where traveltime attributes are used. Traveltime shift between two data sets Δt_{4D} is directly proportional to the 4D velocity difference structure $\Delta v_{4D}(\mathbf{r})$ between two surveys. Thus, combining Eq. (7) with Eq. (9) we account for the single scattering of propagating waves, and with Eq. (13) we integrate only along ray paths when estimating 4D velocity changes in time-lapse

data set. Both theories have their own regime of validity, but finite-frequency wave theory is extension of ray theory and should be used always when condition for ray theory are not satisfied i.e., when media inhomogeneities are smaller in size than λ and L_F.

DESCRIPTION OF THE DURHAM EXPERIMENT

For the physical modeling part, we turn to Durham time-lapse ultrasonic experiment. Our objective is to validate time-lapse crosswell monitoring method using ultrasonic data. Ultrasonic broadband waveform data are recorded in the ultrasonic seismic laboratory at the University of Durham where crosswell seismic survey was simulated [Legget et al. (1993); Pratt (1999)]. The physical model (two of them) in Durham experiment consists of seven layers with different epoxy resin mixtures representing plane-layered sedimentary sequence containing a reservoir layer and simple geological structure. Two models differed only in the reservoir layer, which was in one case uniform (representing pre-flood stage) and in another it contained post-flood zone (simulating progress of fluids injected in reservoir rocks during enhanced oil recovery process). A cross section of the model(s) is illustrated in Fig. 2 where flood zone in the reservoir layer is indicated by cross-hatched region. Photography of physical model prepared for the measurements is shown in Fig. 3, but layered structure is hardly visible and therefore it has been sketched in Fig. 2. Furthermore, Fig. 2 also shows nominal velocities, which are only an indication for the true velocity model since characteristics of epoxy resin are only weak under control. From the practical point of view, the post-flood model in the Durham experiment was obtained by replacing a part of the reservoir layer with an epoxy mixture of lower velocity and greater absorption to simulate a flood zone. The initial reservoir layer (of the epoxy raisin) had the nominal velocity of 2573 m/s while the replaced material had the velocity of 2147 m/s in the post-flooded model. Time-lapse traveltime tomographic imaging technique aims to locate the extent of the flood zone and to accurately detects the velocity change.

Low-frequency transmitted waves were acquired from each model (in a form of two data sets) in a crosswell configuration with two vertical wells. In between the two wells, the velocity model consists of large and small scale structures. For the small-scale velocity structure (thin layer with one channel feature), the theoretical requirements for the application of ray theory are not satisfied. On the contrary, the conditions for the application of finite-frequency wave theory are valid for the complete velocity structure of the epoxy raisin model in the Durham laboratory experiment. However, the difference between two models i.e., the flood zone can be considered as a large scale structure and therefore, it is expected to be imaged well enough both with ray and wave theory based inversion. The ultrasonic surveys also include realistic noise contributions due to uncertainties in source-receiver positions, in the traveltime estimation and in the estimation of the reference velocity, see Legget et al. (1993). Furthermore, two models are used to simulate one configuration at the two separate moments in time (i.e., two different stages) which is also source of some errors. The models were intentionally made to be identical, apart from the flood zone, but that can never be completely achieved.

In the ultrasonic experiment, 500 kHz piezoelectric transducers are used as sources and receivers. There are 51 source and receiver positions which results in 2601 recorded traces. The target zone of velocity between the two wells measures 46.5 mm in the offset direction and 125 mm in the depth direction. To simulate a realistic crosswell experiment,

all distances, times and frequencies are scaled by a factor 1000. Hence, the lateral length and depth of the target zone has the dimensions 46.5 m×125 m, whereas the frequency of the recorded wavefield is between 200 Hz and 500 Hz.

Fig. 4. shows several shot-gathers for pre-flood and post-flood model, in the range where flood zone is located. The changes of velocity structure between two subsequent surveys are reflected in the arrival times of P-waves.

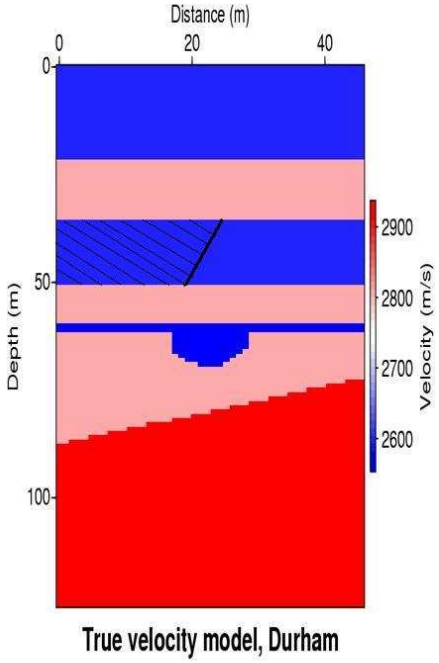

Figure 2: Physical model. Cross section of the epoxy resin scale model with the indication of the nominal velocities. Additionally, the location of the flood zone is presented by the cross-hatched region.

The Durham laboratory experiment makes use of transmitted waves that propagate in 3D. However, the epoxy model represents a 2.5D velocity medium, since the velocity is constant in the lateral direction perpendicular to the source-receiver plane. In turn, the finite-frequency Fréchet kernels for the transmitted waves are derived from the 2D wave equation.

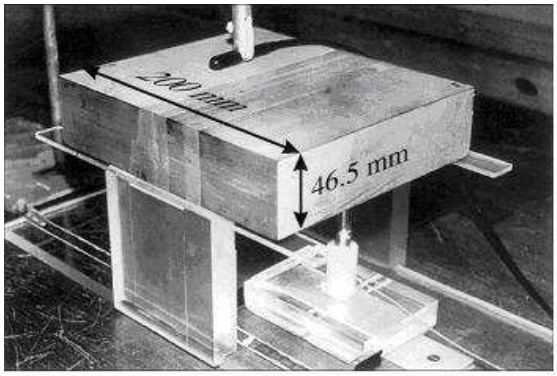

Figure 3: Physical model, made of epoxy raisin, prepared to be immersed in the water for the ultrasonic measurements. Courtesy of Legget.

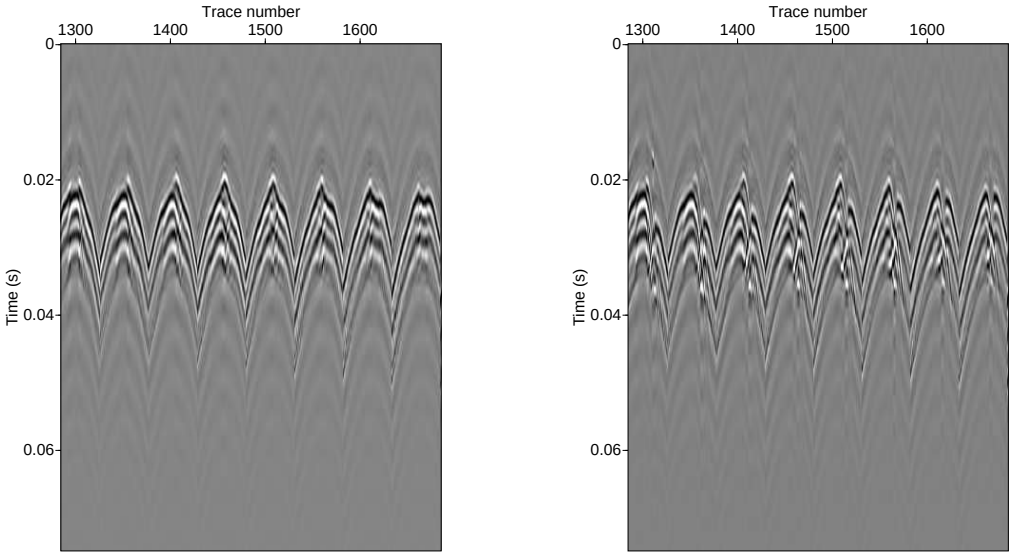

(a) (b)

Figure 4: Recorded wavefields - several shotgathers for pre-flood model and post-flood model: (a) Baseline data, (b) Monitoring data.

2D FINITE-DIFFERENCE MODELING

To complete this validation study, we complement laboratory data with synthetic data simulating ultrasonic experiment. We aim to model ultrasonic wave experiment from Durham, by 2D numerical simulations based on finite-difference (FD) method.

Numerical finite-difference solution of the elastic wave equation is used to compute wavefield similar to the one recorded in the ultrasonic wave experiment. For the discretisation of the elastic wave equations staggered second-order-accurate scheme (Virieux (1992); van Vossen et al. (2002)) is used for both space and time discretisation. Derivatives are discretized using centered finite differences and only two points are needed to estimate spatial derivatives. Spatial sampling is a grid cell 0.5x0.5 m, and Courant number fixes time sampling to $1\mu s$. The geometry of the layered model subjected to this numerical test is identical to the sketch of the model shown in Fig. 2. In comparison to the physical model (Fig. 3) dimensionality is the only difference (3D physical model versus 2D numerical model). Forward modeling is done in two dimensions while waves are propagating in all three dimensions in the ultrasonic experiment. Nevertheless, physical model is considered as 2.5D medium due to the constant velocity in the lateral direction, as it is argued in the section above. All other ultrasonic parameters are preserved in this numerical test. Hence, there is 51 sources and 51 receivers separate by 46.5 m, source (and receiver) array spacing is 2.5 m, depth is 125 m, etc.

As the source function Ricker wavelet is applied. At the receiver positions measured waveforms are bandpass filtered between 100 and 800 kHz.

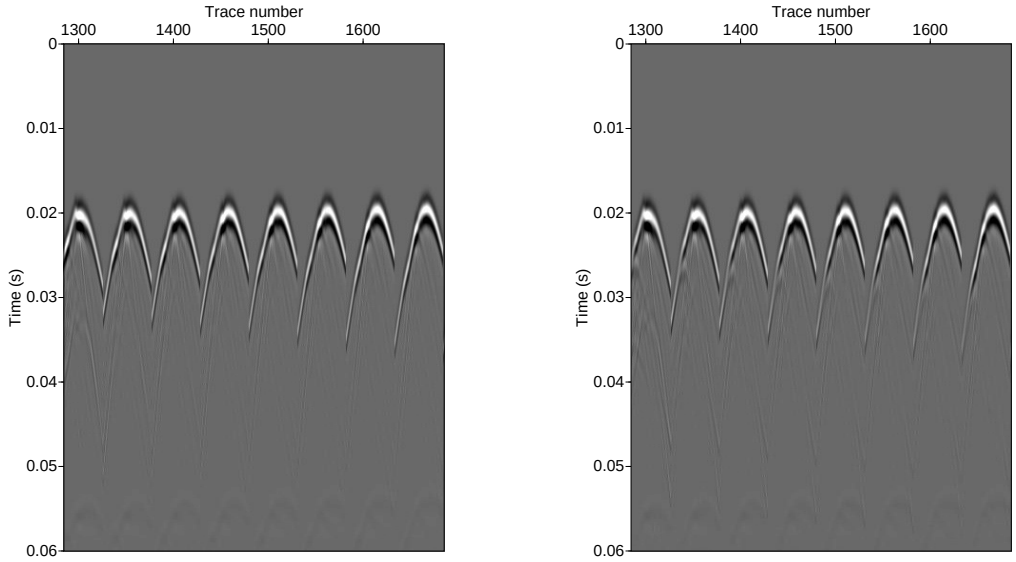

(a) (b)

Figure 5: Synthetic seismograms - several shotgathers for: (a) Baseline data, (b) Monitoring data

Fig. 5 shows several shootgathers of the synthetic seismograms, for the same offset as in Fig. 4 for the recorded ultrasonic data. Fig. 5a represents shootgathers of the baseline model where reservoir layer is homogeneous, and Fig. 5b shows shootgathers for the monitoring model where water has flooded left part of the reservoir. Since in the numerical experiment repeatability of the source-receiver positions is perfect and there is no additional noise, difference between baseline and monitor waveforms seems smaller compared to the recorded waveforms (Fig. 4a and b). Only difference between two subsequent synthetic experiments is introduced by the water flooding the reservoir.

Synthetic experiment is done in order to validate our time-lapse tomographic inversion approach as stable and well-defined. Therefore, processing synthetic and real data files is done at the essentially same way, and results are presented in the next section together with the details of the processing routine.

RESULTS OF TIME-LAPSE TOMOGRAPHY

In this section, we present results of 4D tomographic inversion of synthetic data obtained by 2D FD modeling and real ultrasonic data recorded at Durham.

To locate the flood zone by 4D tomography, there are two equivalent approaches to be applied. One is to perform separate traveltime inversion of data from the baseline survey and data from the monitoring survey, obtain velocity tomograms and then find the difference by subtracting the estimated baseline model from the inverted monitor model. Another approach is to direct invert the traveltime delays between the first arrivals in the pre-flood model and first arrivals in the post-flood model in order to obtain image of the time-lapse velocity structure.

To invert one data set, the following steps are carried out: 1) Define a relevant reference model and calculate Fréchet kernels compiled with either finite-frequency wave theory or ray theory, 2) calculate the reference traveltimes, 3) estimate the traveltime delay between the observed and reference traveltimes, and finally 4) invert the observed traveltime shifts in order to estimate a velocity model between the two wells.

For the time-lapse monitoring, the more direct approach for the inversion consist of one step less. Namely, instead of steps 2) and 3) there is only one: the estimation of the traveltime shift between the baseline and monitor traveltimes. That has been obtained automatically by the cross-correlation of the recorded waveforms (previously muted and filtered) from the baseline and monitoring survey.

We test our 4D methodology using described direct method on the synthetic data. The inversion is compiled with ray theory and finite-frequency wave theory for the sake of comparison. Results are presented in the Fig. 6 (a and b). Time-lapse tomograms are of excellent quality which validated use of our 4D monitoring technique. We observe only a small difference between two images of Fig. 6 which are compiled by two different theories. This is expected since the conditions for ray theory are not violated considering the length-scale of detected flood-zone.

In the processing of ultrasonic data and synthetic data, we used same reference model. The reference velocity model is obtained assuming that calibrated sonic logs were run in both wells to give an initial estimate of the velocity field between the two wells in a baseline

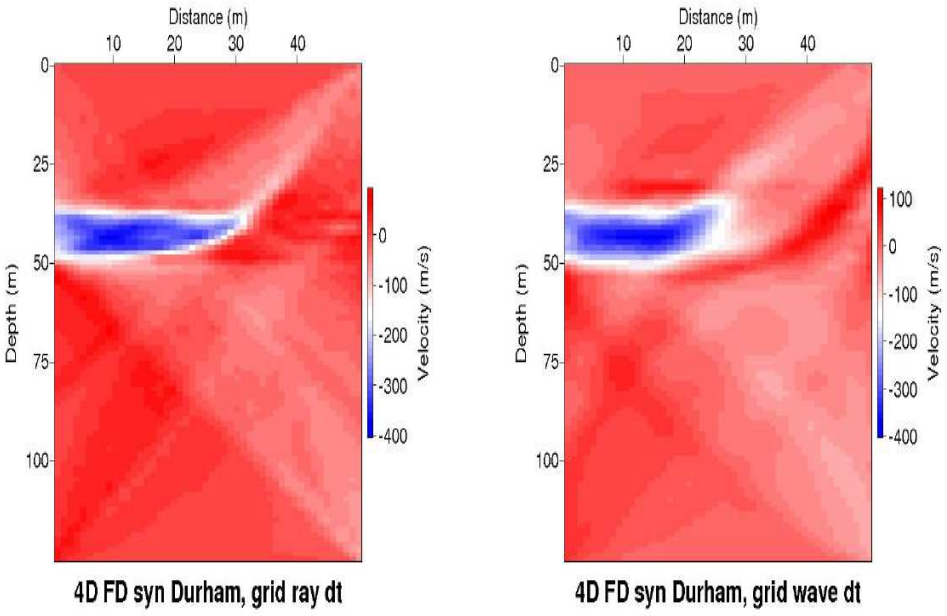

(a) (b)

Figure 6: Validation of time-lapse tomogrphy using synthetic data. 4D images are compiled by: (a) Ray theory, (b) Scattering theory.

survey (i.e., by the linear interpolation). Therefore, we have used the velocity structure in Fig. 2 only without the thin layer with the channel structure. The parameterisation of the velocity model is a grid by 64×24 cells of the constant velocity (used both in processing synthetic and ultrasonic data). The Fréchet kernels with respect to the reference model are computed either with scattering theory or ray theory. For the inversion of only one data set, the traveltime delay is estimated as the difference between the observed traveltimes and the reference traveltimes. The reference traveltimes are always calculated for the reference model with ray theory. To compute the observed traveltime delay, reference traveltimes are subtracted from the observed traveltimes. The observed traveltimes are estimated in a correlation analysis of the observed waveforms and the source wavelet where the latter is known from an independent measurement in water.

Finally, a common least-squares inversion method is applied in the finite-frequency wave and ray theoretical inversion. It is fair to compare the estimated velocity models compiled with scattering theory and ray theory only when the resolution matrices in the these two different inversion approaches are identical. As has been previously shown by Spetzler (2003a,b), the velocity tomogram compiled by wave theory is with higher resolution compared to the one obtained with ray theory. In addition, because of the limitations of the high-frequency approximation applied in ray theory, the strength of small-scale velocity is underestimated. The breakdown of ray theory is as well clearly demonstrated in Figs. 4 and 5 of Spetzler and Snieder (2001).

As the result of processing ultrasonic lab data, we show the time-lapse velocity tomograms compiled with the finite-frequency wave theory and the standard ray theory in Fig. 7a and 7b, respectively. The result presented in Fig. 7 is a difference tomogram using traveltime shift obtained from pre-flood and post-flood traveltimes cross-correlation and then inverted by method based on ray theory. Fig. 7a gives result for the same traveltime shift data but now inverted using sensitivity kernels computed by wave theory. We observe only a small difference between these two images in Fig. 7. Still, the time-lapse velocity tomogram obtained by the finite-frequency wave theory seems to be overall less noisy.

We estimate from synthetic and ultrasonic experiment that the time-lapse velocity change in the reservoir layer is on the order of -400 m/s which is in agreement with the reality. Thus, our time-lapse method gives an accurate estimation of the induced velocity difference. Also, the front of the flooding zone is accurately located.

Fig. 8c shows a difference velocity tomogram obtained simply by subtracting the pre-flood image Fig. 8a from the post-flood image Fig. 8b. Those two images (Fig. 8a and 8b) were estimated separately by tomographic inversion following four-step procedure previously decribed. The finite-frequency wave theory was used in the inversion step. The time-lapse tomographic velocity field is consistent with the one in Fig. 7, but shows much more noise and some additional differences. That is a consequence of two separate and independent inversions where not all parameters and characteristics of the inversions are necessarily the same. The damping parameter is different in order to get similar velocities and consequently, it is difficult to obtain identical chi squared values (the chi squared value is a combination of the data misfit and the model resolution). The 4D result is affected by the velocity differences in the other parts of the model since finite-frequency inversion is more sensitive than the ray theory to preprocessing errors in the observed data. Also, the velocity difference in the flood zone is slightly underestimated.

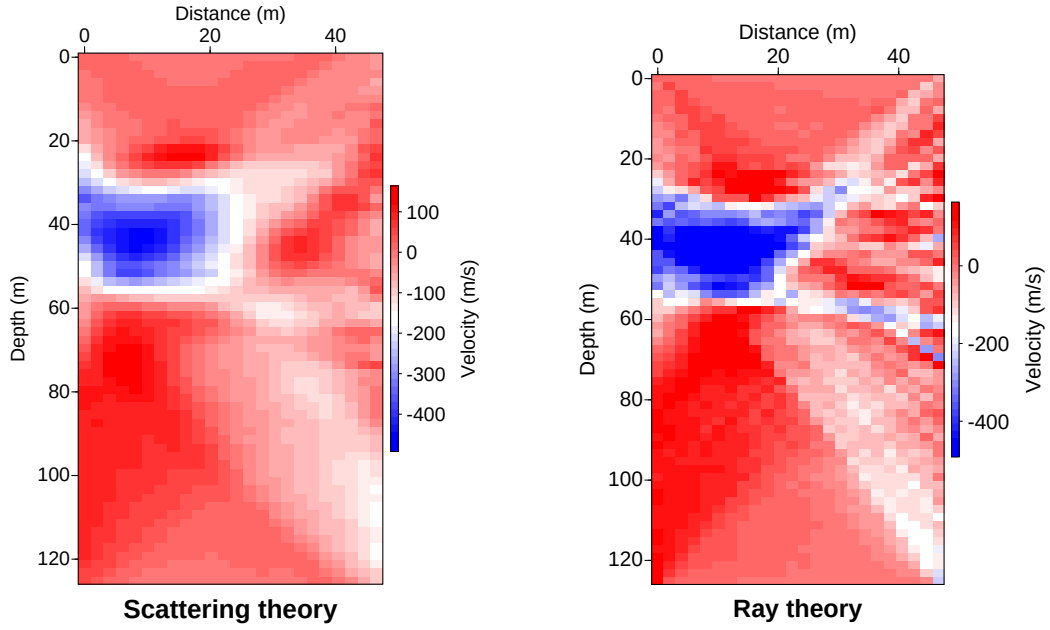

(a) (b)

Figure 7: Time-lapse result of traveltime delay tomographic inversion. (a) Velocity difference structure compiled from scattering theory. (b) Velocity difference structure inferred from ray theory.

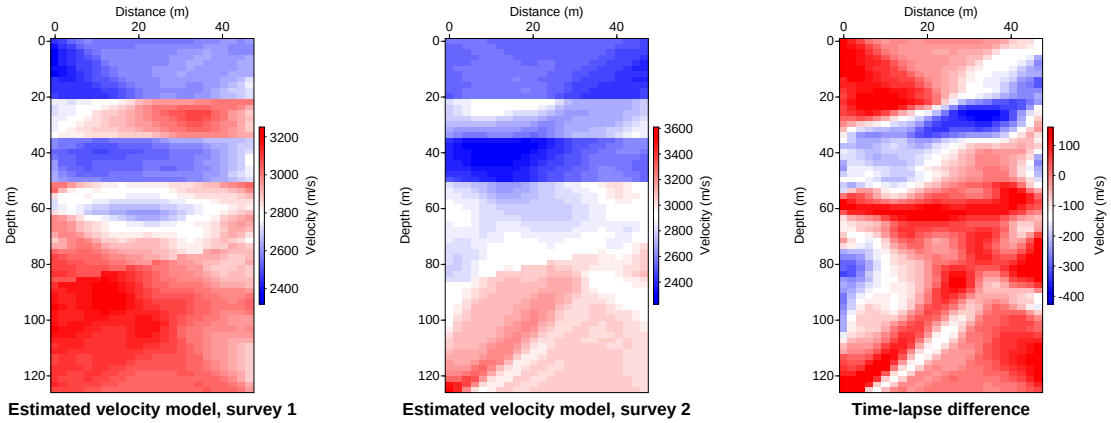

(a) (b) (c)

Figure 8: Standard time-lapse approach.(a) Velocity tomogram of a baseline survey, (b) Velocity tomogram of a monitoring survey, (c) Difference velocity tomogram formed by subtracting baseline (pre-flood) image from the post-flood image.

DISCUSSION AND CONCLUSIONS

Using synthetic data and real ultrasonic data, we show that traveltime time-lapse tomography is a powerful method for monitoring and might have a number of applications.

We proposed to apply a finite-frequency wave theory in time-lapse tomographic inversion scheme, since it is not affected by the limitations of ray theory. In the contrast to wave theory, ray theory is not valid for the media where the size of the velocity anomalies is smaller than the Fresnel zone.

In the Durham time-lapse ultrasonic experiment, both ray and wave theory give satisfactory estimations of the flood zone in the reservoir (since its size is larger than the Fresnel zone). The process of the traveltimes shift estimation plays an important role. Our conclusion is that traveltime shift should be estimated in the cross-correlation of muted data from the baseline and monitoring survey. After that moving average filter should be applied on the estimated time shifts. Inverting data file produced in such a way result with the image free of noise in which the accurately located flood zone has relatively sharp edges (for the synthetic data see Fig. 6, and for ultrasonic see Fig. 7).

Time-lapse tomography combined with the finite-frequency wave theory is applicable in some other geophysical disciplines, such as high-resolution reservoir characterisation, fluid front detection and monitoring of CO_2-sequestration. Recently, it has been applied successfully to monitor steam injection into the tar send in Alberta region, and in Japan to monitor injection of CO_2 into the sand aquifer. Currently, we are preparing scaled ultrasonic experiment for the simulation of CO_2 injection in the subsurface (Šijačić et al. (2006)). The time-lapse tomographic method will be applied to monitor induced velocity changes.

FORECAST OF ACTIVITIES WITHIN WP 5:

- Apply the same 4D methodology to monitor injection of CO_2 into the coal layer. Physical model of the RECOPOL configuration is already made and the next step is to record ultrasonic data in the crosswell acquisition. Due to the failure of the equipment, measurements are delayed but the first results are expected for the February 2007.

REFERENCES

Aki, K. and P. G. Richards, 1980, Quantitative seismology: Theory and methods: W. H. Freeman and Co.

Legget, M., N. R. Goulty, and J. E. Kragh, 1993, Study of traveltime and amplitude time-lapse tomography using physical model data: Geophys. Prosp., **415**, 599–619.

Pratt, G. R., 1999, Seismic waveform inversion in the frequency domain, part 1: Theory and verification in a physical scale model: Geophysics, **64**, 888–901.

Snieder, R. and A. Lomax, 1996, Wavefield smoothing and the effect of rough velocity perturbations on arrival times and amplitude: Geophys. J. Int., **125**, 796–812.

Snieder, R. and M. Sambridge, 1992, Ray perturbation theory for traveltimes and ray paths in 3-d heterogeneous media: Geophys. J. Int., **109**, 294–322.

Spetzler, J., 2003a, Comparison of ray theory and finite-frequency wave theory in crosswell tomography: Presented at the 65th, EAGE.

——— 2003b, Finite-frequency wavefield theory for high-resolution velocity estimation using transmission and reflection data: 73rd, Expanded Abstracts, 2315–2318, Soc. of Expl. Geophys.

Spetzler, J. and R. Snieder, 2001, The effects of small-scale heterogeneity on the arrival time of waves: Geophys. J. Int., **145**, 786–796.

van Vossen, R., J. O. A. Robertsson, and C. H. Chapman, 2002, Finite-difference modeling of wave propagation in a fluid-solid configuration: Geophysics, **67**, 618–624.

Virieux, 1992, blablabla: Geophysics, **57**, 15–26.

Šijačić, D., J. Spetzler, and K. Wolf, 2006, Acoustic monitoring of co_2/methane migration in coal seams: , 15 pages, International coalbed methane simposium.

Woodward, M. J., 1992, Wave-equation tomography: Geophysics, **57**, 15–26.